



THE UNIVERSITY *of* EDINBURGH

Edinburgh Research Explorer

A SERS-Active Electrospun Polymer Mesh for Spatially Localized pH Measurements of the Cellular Microenvironment

Citation for published version:

Skinner, WH, Chung, M, Mitchell, S, Akidil, A, Fabre, K, Goodwin, R, Stokes, AA, Radacsi, N & Campbell, CJ 2021, 'A SERS-Active Electrospun Polymer Mesh for Spatially Localized pH Measurements of the Cellular Microenvironment', *Analytical Chemistry*. <https://doi.org/10.1021/acs.analchem.1c02530>

Digital Object Identifier (DOI):

[10.1021/acs.analchem.1c02530](https://doi.org/10.1021/acs.analchem.1c02530)

Link:

[Link to publication record in Edinburgh Research Explorer](#)

Document Version:

Peer reviewed version

Published In:

Analytical Chemistry

General rights

Copyright for the publications made accessible via the Edinburgh Research Explorer is retained by the author(s) and / or other copyright owners and it is a condition of accessing these publications that users recognise and abide by the legal requirements associated with these rights.

Take down policy

The University of Edinburgh has made every reasonable effort to ensure that Edinburgh Research Explorer content complies with UK legislation. If you believe that the public display of this file breaches copyright please contact openaccess@ed.ac.uk providing details, and we will remove access to the work immediately and investigate your claim.



A SERS-active electrospun polymer mesh for spatially localized pH measurements of the cellular microenvironment

William H. Skinner,^{‡1} Michael Chung,^{‡2} Stephen Mitchell³, Asli Akidil⁴, Kristin Fabre,⁵ Richard Goodwin⁴, Adam A. Stokes², Norbert Radacsi², Colin J. Campbell^{*1}

¹ EaStCHEM School of Chemistry, University of Edinburgh, The University of Edinburgh, King's Buildings, Mayfield Road, Edinburgh EH9 3FJ, United Kingdom

² School of Engineering, The University of Edinburgh, King's Buildings, Mayfield Road, Edinburgh EH9 3JL, United Kingdom

³ School of Biological Sciences, The University of Edinburgh, EH9 3BF, United Kingdom

⁴ Clinical Pharmacology and Safety Sciences, Biopharmaceuticals R&D, AstraZeneca, Cambridge, CB4 0WG, United Kingdom

⁵ Innovation Scientist, Baylor College of Medicine, Centre for Space Medicine, Houston, Texas, TX 77030, USA

*Corresponding Author: colin.campbell@ed.ac.uk

ABSTRACT: Extracellular pH (pHe) is an important chemical factor in many cellular processes and disease pathologies. The routine sampling of pHe *in-vitro* could lead to innovative advances in therapeutics. To this end, we have fabricated a novel gold-coated polymer mesh which facilitates the real-time measurement of pHe via surface-enhanced Raman scattering (SERS). In this proof of concept study, we apply our SERS sensor to measure metabolically-induced changes in the pHe of carcinoma-derived cell line HepG2/C3A. We demonstrate that gold-coated polyurethane electrospun nanofibers (AuNF) have strong and reproducible SERS spectra of surface adsorbed analytes. By functionalizing AuNF with pH-responsive reporter 4-mercaptobenzoic acid (MBA), we have developed an accurate pH SERS sensor for the extracellular microenvironment. We cultured HepG2/C3A on the surface of MBA-AuNF and measured an acidic shift in pHe at the cell-fiber interface. Following exposure to staurosporine, an apoptosis-inducing drug, we observed changes in HepG2/C3A cellular morphology indicative of controlled cell death, and detected an increase in the pHe of HepG2/C3A. These results demonstrate how subtle changes in pHe, induced by the metabolic activity of cells, can be measured with our novel SERS sensor MBA-AuNF. The excellent pH measurement performance of MBA-AuNF provides a unique platform to study extracellular pH on the microscale and will help to deepen our understanding of pHe in disease pathology.

The extracellular pH (pHe) of tissue is a key regulating factor in the physiological activity of cells.¹ Aberrant pHe in the cellular microenvironment is implicated in the progression of diseases such as cancer and cystic fibrosis.²⁻⁴ However, the pHe of the cellular microenvironments *in-vitro* is challenging to measure, because of the microscale of the sensing target and the spatial targeting requirements of the sensor. To this end, there is a need to develop a facile means to measure the pHe of cell cultures *in-vitro*.

The sensing methods used to measure pH *in-vivo* are not easily applied to *in-vitro* cell culture. Magnetic resonance imaging (MRI) is used to measure pHe in tissue, but has limited spatial resolution and is not suitable for the high throughput analysis required for *in-vitro* cell cultures.⁵ The use of pH electrodes to measure pHe *in-vitro* is also limited, due to the technical feasibility of positioning the probe in the cellular microenvironment.

Fluorescence-based pH-sensitive molecular probes are a well-established means of measuring intracellular pH *in-vitro*. However, to measure pHe these molecular probes must be retained on the cell surface, without being internalized by the cell or diffusing away.⁶ Cell-surface-anchored probes, employing low pH insertion peptides and streptavidin-biotin interactions, have been developed to overcome this challenge.⁷⁻⁸ These approaches are limited because their application is complex, and the probe-cell anchors have the potential to disrupt cell physiology and induce adverse biological responses.⁶

Recently plasmonic nanostructured cell culture platforms have been developed to measure pHe using surface-enhanced Raman spectroscopy (SERS).⁹⁻¹⁰ Raman spectroscopy is a rapid, non-invasive spectroscopic technique that enables fingerprinting of biological and chemical samples. SERS enhances the intensity of the Raman fingerprint of molecules in proximity to plasmonic nanostructures¹¹ and has several advantages over

fluorescence, including multiplexed detection, low autofluorescence, and resistance to photobleaching.¹²⁻¹³ Furthermore, SERS requires the molecular probe to be anchored to a solid phase plasmonic substrate. If the size of this substrate is designed to be too large for the cells to endocytose the sensor will be restricted to the extracellular space with no risk of cell internalization. These characteristics make SERS-active cell culture platforms excellent candidates for non-invasive *in-situ* pH monitoring of the cellular microenvironment.

SERS substrates for pH sensing have been fabricated with electron-beam lithography and metallic nanoparticle assemblies.⁹⁻¹⁰ Functionalizing these plasmonic substrates with pH-sensitive Raman reporter molecules 4-mercaptobenzoic acid (MBA) or mercaptopyridine (MPY) facilitates pH measurements at the substrate surface with Raman spectroscopy. pH SERS substrates have been used to support *in-vitro* cell cultures and distinguish differences in local pH between tumor cell lines and normal cell lines.⁹⁻¹⁰

In this paper, we present a novel SERS active substrate, gold-coated polyurethane electrospun nanofibers (AuNF), and apply it to measuring the pH of *in-vitro* cell cultures. We fabricate polyurethane nanofibers using a “benchtop” process called electrospinning. By sputter coating the fibers with gold, we leverage the inherent nanoscale architecture of the fibers to create a plasmonic substrate, AuNF, for SERS pH sensing.¹⁴ This two-step fabrication process is low cost and does not require specialist photolithographic technologies, or colloidal nanoparticles, which are typically used to create SERS substrates for pH sensing.^{9, 15-16} Furthermore, the advent of high-throughput electrospinning, and the low cost and simplicity of the process we document, make AuNF a pH SERS substrate well suited to fabricate at scale.¹⁷

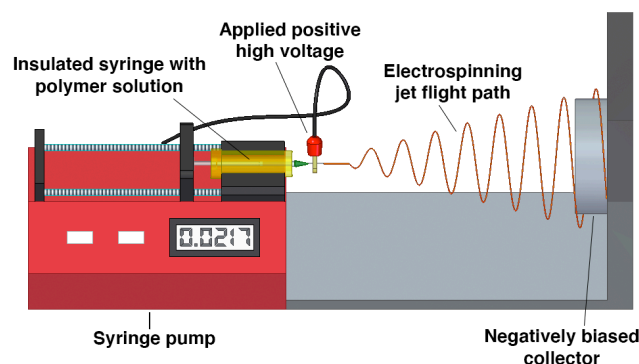
In a conventional electrospinning setup, a polymer solution is loaded into a syringe and a large potential difference is applied between the syringe and a target (Scheme 1). When the surface tension barrier of the polymer solution is overcome, a thin jet of solution spirals towards the negatively biased collector.¹⁴ The solvent evaporates during this flight, and dry polymer fibers are collected on the target. These electrospun polymer fibers have high surface-volume ratios and controllable material properties which make them suitable for applications in sensing, cell culture, and wound healing scaffolds.¹⁸⁻¹⁹ Extracellular matrices for a range of tissues have been developed by controlling fiber thickness and mesh density.¹⁹⁻²¹

A widely used method of creating SERS substrates from electrospun nanofibers is to decorate the fibers with metallic nanoparticles.^{16, 22} We demonstrate that, in the absence of nanoparticles, gold-coated polyurethane nanofibers yield a strong SERS enhancement suitable for *in-situ* pH sensing. This simplifies the substrate fabrication process, removing the need for technically challenging nanoparticle synthesis and removing the risk of nanoparticle leaching. Nanoparticle leaching could lead to endocytosis and the inadvertent measurement of intracellular pH instead of pH_e.²³

In this study, we functionalized AuNF with MBA (MBA-AuNF) and created a SERS active cell culture platform that could monitor pH_e in the cellular microenvironment. MBA-AuNF had excellent pH sensitivity between pH 6 and 8, which was spatially consistent over the fiber substrate. To demonstrate the biomedical sensing application of MBA-AuNF, we cultured HepG2/C3A cells on the fiber surface and measured an acidic pH_e at the cell-fiber interface. We then treated the HepG2/C3A

cells with nonspecific protein kinase inhibitor staurosporine (STS) and measured an increase in local pH_e simultaneous to changes in cell morphology which are associated with apoptosis. This demonstrates the potential of MBA-AuNF as a tool to investigate the relationship between intracellular processes and pH_e.

Scheme 1. Electrospinning Apparatus



EXPERIMENTAL SECTION

AuNF fabrication. We used polydimethylsiloxane (PDMS) as a flexible and transparent support to electrospin polyurethane fibers onto. We prepared the PDMS (Sylgard 184) by adding the catalyst to the base reagent at a weight ratio of 1:10. We poured this mixture into a mold to a depth of 0.5 mm and cured it for 1 h at 100 °C. We then cut the PDMS into sheets of 30 x 60 mm, into which rows of 6 mm holes were cut at 1 cm intervals using a biopsy punch. This allowed access to the negatively biased electrospinner collector through the electrically insulating PDMS film and facilitated the collection of fibers on the surface of the PDMS between the holes (Figure S1).

We prepared 10 mL of electrospinning solution by adding 1.8 g of thermoplastic polyurethane (TPU) to 8.2 mL of dimethylformamide (DMF). The TPU solution was mixed with a magnetic stirrer for 24 hr at an RPM of 200, at 80 °C, after which we added 50 μ L of 37% hydrochloric acid to the TPU solution. We used a horizontal needle electrospinning setup (IME Medical Electrospinning, Netherlands) to fabricate the fibers. The TPU solution was added to a 1 mL syringe with a 21G (0.8 mm diameter) blunt needle, and placed in a syringe pump set at a flow rate of 5 μ L \cdot min⁻¹. The PDMS sheet, described above, was placed on the metallic collector set at a distance of 20 cm away from the needle tip. We applied a positive voltage of 20 kV to the needle and biased the collector to -4 kV. During electrospinning the ambient temperature was 20-23 °C and the relative humidity was between 30-40%. We electrospun the TPU onto the PDMS for 5 minutes to obtain an ultrathin layer of polyurethane fibers on the PDMS surface (Figure S1). The fibers, supported by PDMS, were coated with 30 nm of gold using an automatic sputter coater (Agar Scientific Ltd., UK) with a 57 mm diameter gold target. We checked fiber morphology using a JSM-IT100 scanning electron microscope (SEM) (JEOL Ltd., Japan). Mean fiber diameter was calculated using ImageJ software by taking 50 diameter measurements from two separate 2000X magnification SEM images.

Following the application of the gold layer, we cut the PDMS-mounted fiber samples (AuNF) into 2.5x2.5 mm squares with a surgical scalpel.

Biocompatibility of AuNF. We incubated AuNF in a solution of collagen (100 $\mu\text{g/ml}$) in phosphate buffer solution (PBS) (NaCl 137 mM, KCl 2.7 mM, Na_2HPO_4 10 mM, KH_2PO_4 1.8 mM) for 2 hr at 37 °C and then seeded HepG2/C3A cells onto the AuNF at 3.1×10^4 cells/ cm^2 . We measured the relative increase in the number of viable cells between 20 hr and 63 hr after seeding with ATP assay CellTiter-Glo® (Promega). Luminescence was measured using a SpectraMax M5 plate reader (Molecular Devices) and an exposure time of 0.5s.

AuNF surface modification. We immersed the AuNF in a 100 μM solution of MBA in 1% ethanol (EtOH) in deionized water (DI), and incubated it for 24 hours at 8 °C. The following day we washed the MBA-AuNF with $\times 1$ 70% EtOH in DI, and $\times 2$ PBS.

MBA-AuNF pH calibration. We calibrated the MBA-AuNF pH sensors by collecting SERS spectra from the fiber surface at pH 5–8. We used Specpure® buffers for pH 5, 6, 7, and 8, and phosphate buffer saline solution for pH 7.2 and 7.4. For each pH in the calibration curve, we collected 9 SERS spectra (Figure S2), from 3 random areas, on 3 MBA-AuNF substrates. All spectra were collected using the Renishaw InVia Raman spectroscope, with a $60 \times$ N.A. = 1 water immersion objective and 785 nm laser. For spectral acquisitions, we used 0.5 mW laser power and 2s acquisition time. We processed all spectra with 9 points Savitsky-Golay smoothing (polynomial order 3), and baseline subtraction, with the WiRe™ intelligent fitting function. We calculated the intensity ratio of the MBA carboxylic acid peak ($\nu_s(\text{COO})$) at $\sim 1400 \text{ cm}^{-1}$ and the ring deformation mode ($\nu(\text{ref})$) at $\sim 1590 \text{ cm}^{-1}$ for each spectrum using a bespoke MatLab code. Origin™ was used to plot the calibration data and fit a Boltzmann curve.

We validated our MBA-AuNF pH calibration curve by collecting Raman maps from MBA-AuNF in buffers at pH 6, 7, 7.4 and 8, and calculating pH from the spectra. We collected Raman spectra at 10 μm intervals in a $80 \times 90 \mu\text{m}$ area on the MBA-AuNF surface, with the same Raman microscope settings used for pH calibration. We used the pH calibration curve to calculate pH from the intensity ratio of $\nu_s(\text{COO})$ and $\nu(\text{ref})$ in each MBA-AuNF spectrum.

Cell culture on MBA-AuNF. We cultured HepG2/C3A up to passage 10 in collagen-coated flasks in Dulbecco's Modified Eagle Medium (DMEM), high glucose, with 10% fetal bovine serum and 1% penicillin-streptomycin.

We prepared MBA-AuNF for cell culture by sterilizing the fibers with 70% EtOH in DI and washing $\times 2$ with PBS. The MBA-AuNF were then incubated in a solution of 100 $\mu\text{g/ml}$ of collagen (type 1) in PBS for 2 hr at 37 °C, following which we seeded HepG2/C3A, at 2×10^5 cells/ cm^2 , onto the MBA-AuNF. We cultured the cells on MBA-AuNF for 24 hr at 37 °C and 5% CO_2 before collecting pH measurements.

Cell fixing for SEM. We fixed HepG2/C3A cultures, on MBA-AuNF, in a solution of 3% glutaraldehyde in 0.1 M sodium cacodylate buffer (pH 7.3) for 2 hours. The cells were then washed in 3 \times 10-minute changes of 0.1 M sodium cacodylate buffer. We postfixed the samples in 1% osmium tetroxide in 0.1 M sodium cacodylate buffer for 45 minutes. We then performed 3 \times 10-minute washes of the sample in 0.1 M sodium cacodylate buffer. We dehydrated the cells in graded concentrations of acetone (50%, 70%, 90%, and 3 \times 100%) for 10 minutes each, followed by critical point drying using liquid carbon dioxide. We mounted the samples on aluminum stubs for sputter coating

with 20 nm gold and imaged the cells using a JSM-IT100 scanning electron microscope (SEM) (JEOL Ltd., Japan).

HepG2/C3A pH measurements. We analyzed MBA-AuNF 24hr after cell seeding, at which point a confluent layer of HepG2/C3A had formed on the MBA-AuNF surface. For spectral acquisition, the cells were washed ($\times 1$) and submerged in a PBS imaging solution (NaCl 137 mM, KCl 2.7 mM, Na_2HPO_4 1 mM, KH_2PO_4 0.18 mM). We collected spectra from each sample for a maximum of 10 minutes, using the same microscope and laser settings we used for MBA-AuNF pH calibration. We collected nine MBA SERS spectra (Figure S3) from three $100 \times 150 \mu\text{m}$ areas on 3 MBA-AuNF with confluent layers of HepG2/C3A. We used the pH calibration curve to calculate pH from the intensity ratio of $\nu_s(\text{COO})$ and $\nu(\text{ref})$ in each MBA-AuNF spectrum.

pH measurements after staurosporine exposure. HepG2/C3A were seeded onto MBA-AuNF as previously described. 24hr after cell seeding, we treated three MBA-AuNF cell cultures with 1 μM of staurosporine (STS) in a solution of 0.01% dimethyl sulfoxide (DMSO) in DMEM. As a vehicle control, we treated three MBA-AuNF cell cultures with a solution of 0.01% DMSO in DMEM. Following 3 hours of incubation, we washed ($\times 1$) and submerged the cultures in PBS imaging solution for spectral acquisition. We collected spectra from each sample for a maximum of 10 minutes, using the same microscope and laser settings we used for MBA-AuNF pH calibration. Nine MBA SERS spectra were collected, (Figure S3), from five different $100 \times 150 \mu\text{m}$ areas, on three control and three STS treated MBA-AuNF substrates supporting confluent layers of HepG2/C3A.

We used bright-field microscope images of HepG2/C3A cultured on MBA-AuNF to quantify cell rounding after STS and vehicle control treatment (Figure S4). Using ImageJ, we manually highlighting > 230 cells in samples exposed to each condition and calculated the roundness of each cell with the ImageJ roundness function.²⁴

Fluorescence staining. We seeded HepG2/C3A onto a 96 well plate at 20,000 cells/well, and after 24hr treated selected wells with 1 μM STS or vehicle control for 3 hours. We then fixed the cells with 4% formaldehyde for 30 minutes at room temperature. We washed and permeabilized the cells with 0.1% Triton X in a 2% BSA PBS solution, and incubated the sample overnight in 2% BSA PBS solution. After washing, we treated the cells for 2 hours with Phalloidin-488 (1 : 500, Thermofisher) and Hoechst 33342 (1 : 1000, Invitrogen) in 2% BSA PBS solution.

Confocal Image Acquisition. We imaged the stained HepG2/C3A cells with Cell Voyager 7000 (CV7000, Yokogawa Inc.), and captured confocal fluorescent images using a long working distance $20\times$ objective (Olympus LUCPLFLN 0.45 NA, WD 6.6–7.8 mm) and an Andor Neo sCMOS camera with a 1×1 bin. We imaged Hoechst using a 405 nm excitation laser ($405 \pm 5 \text{ nm}$, 100 mW, Coherent) with a 445/45 nm bandpass emission filter and imaged Phalloidin using a 488 nm excitation laser ($488 \pm 2 \text{ nm}$, 200 mW, Coherent) with a 525/50 nm bandpass emission filter. Images were captured over a 10 μm range at 2 μm Z intervals.

RESULTS AND DISCUSSION

Substrate characterization. SERS substrates for integrated pH sensing *in-vitro* must be optically transparent, biocompatible, and have a strong SERS response. We utilized thin sheets

of AuNF, supported by PDMS, as SERS active substrates to host cell growth and position the AuNF in the cellular microenvironment. Polyurethane nanofibers are biocompatible and well suited to mimicking the cellular microenvironment.²⁵ The fibers in our AuNF substrate had a mean diameter of 352 ± 98 nm (Figure 1a). We confirmed the sustained viability and proliferation of HepG2/C3A cells cultured on AuNF by conducting ATP assay CellTiter-Glo® at 20 hr and 63 hr and measured a relative increase in the cell population. (Figure S5) Furthermore, our use of PDMS as structural support for fibers ensured that the AuNF film remained thin enough to be transparent, allowing the use of a standard bright-field microscope to monitor cells growing on the AuNF surface (Figure 1b).

The gold-coated nano-fibers in AuNF are SERS active. MBA self-assembled monolayers (SAMs) exhibited a strong SERS effect when adsorbed to AuNF, compared to Au directly sputter-coated onto PDMS in the absence of nanofibers (Figure 1c). This confirms that the gold-coated polyurethane nanofibers facilitate the strong SERS signal observed in Figure 1c.

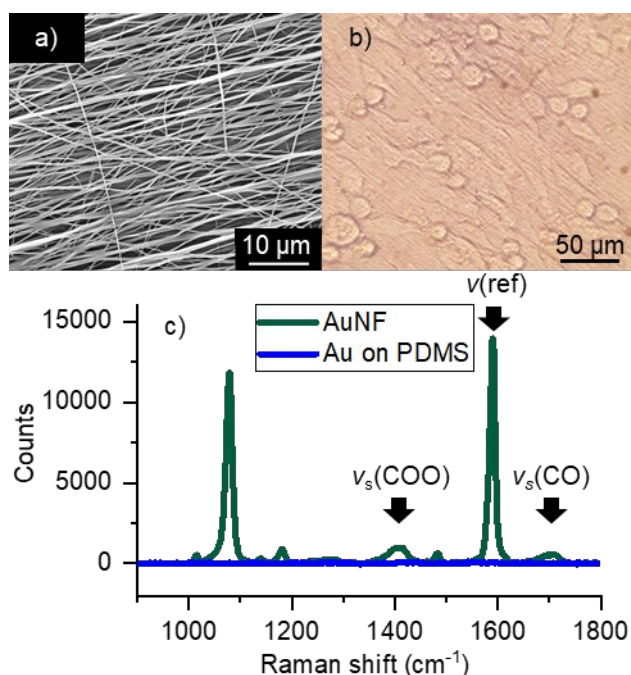


Figure 1. (a) $\times 2000$ SEM image of AuNF. (b) HepG2/C3A cells growing on AuNF. (c) Raman spectrum of MBA adsorbed to AuNF, and Au on PDMS.

In Figure 1c, we assigned the Raman peaks at ~ 1420 cm^{-1} and ~ 1700 cm^{-1} to the symmetric carboxylate vibration ($\nu_s(\text{COO})$) and the carbonyl stretch ($\nu_s(\text{CO})$) of MBA. The intensity of $\nu_s(\text{COO})$ ($I[\nu_s(\text{COO})]$) and $\nu_s(\text{CO})$ ($I[\nu_s(\text{CO})]$) depends on the population of protonated and deprotonated MBA molecules. We assigned the peak at 1590 cm^{-1} to the ring deformation vibration of the MBA aromatic ring ($\nu(\text{ref})$) and used it as a reference against which to normalize MBA spectra for pH sensing.²³ Normalizing the spectra to the intensity of $\nu(\text{ref})$ ($I[\nu(\text{ref})]$) allowed us to correlate $I[\nu_s(\text{COO})]$ with pH at the MBA-AuNF surface. In this work, we utilized $I[\nu_s(\text{COO})]$ for the pH sensor because it increases to 18% of the $\nu(\text{ref})$ intensity, while $I[\nu_s(\text{CO})]$ only increases to $\sim 10\%$ of the $\nu(\text{ref})$ intensity (Figure 2a). This renders $I[\nu_s(\text{COO})]$ more sensitive to pH and a better peak for pH sensing.

pH calibration and sensing with MBA-AuNF. We collected the SERS spectrum of MBA-AuNF between pH 5 and 8, and normalized each spectrum to the intensity of the $\nu(\text{ref})$ peak at 1590 cm^{-1} (Figure 2a). This pH range encompasses the expected pHe of biological tissue.²⁶ The pH-sensitive $\nu_s(\text{COO})$ peak increases in intensity as the pH of the solution increases and the proportion of deprotonated carboxylate groups at the MBA-AuNF surface increases.

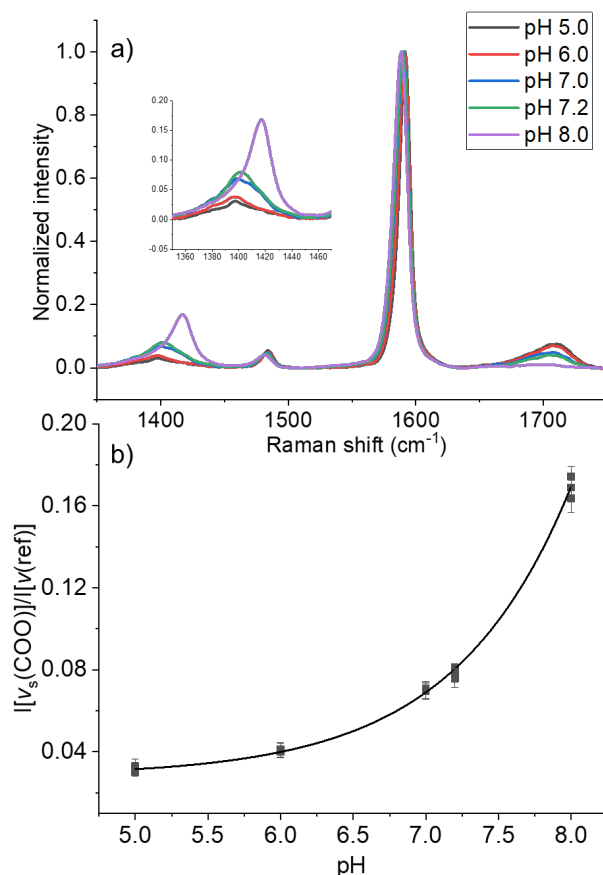


Figure 2. (a) SERS spectrum of MBA-AuNF at pH 5-8, normalized to $\nu(\text{ref})$. (b) $I[\nu_s(\text{COO})]/I[\nu(\text{ref})]$ at pH 5-8, 3 MBA-AuNF samples analyzed at each pH, each data point represents the mean \pm SD of 27 spectra collected at different locations on 3 MBA-AuNF samples.

A plot of pH vs the ratio of $I[\nu_s(\text{COO})]/I[\nu(\text{ref})]$ within a biologically meaningful range is presented in figure 2b. We fitted a Boltzmann curve to these data with good precision, the use of the Boltzmann curve to describe the pH dependence of $I[\nu_s(\text{COO})]/I[\nu(\text{ref})]$ has been established by other publications.^{23, 27} The low standard deviation and dispersion between data points at each pH in figure 2b confirmed that the $I[\nu_s(\text{COO})]/I[\nu(\text{ref})]$ ratio was consistent and reproducible across the pH range.

We collected Raman maps at the surface of MBA-AuNF at pH 6, 7, 7.4, and 8 to demonstrate the uniformity of microscale pH measurements with MBA-AuNF (Figure 3). The 90×80 μm Raman maps were created by collecting MBA-AuNF spectra at 10 μm intervals on the substrate surface. We calculated the pH value for each pixel using the calibration curve in Figure 2b.

Figure 3 highlights the microscale spatial uniformity of pH measurements collected using MBA-AuNF. The standard deviation across the 72 pH pixels was greatest at pH 6, with an SD

of ± 0.25 (Table.1). We attribute this reduced accuracy at pH 6 to the relatively low intensity of $\nu_s(\text{COO})$ at pH 6, $\sim 4\%$ of $I[\nu(\text{ref})]$, and the shallow gradient of the Boltzmann calibration curve in this pH region (Figure 2b). The accuracy of the sensor increased as the pH, and therefore $I[\nu_s(\text{COO})]$, increased. MBA-AuNF accuracy improved significantly at pH 7, where pixel pH had a standard deviation of ± 0.08 pH units. We anticipate that extracellular pH measurements will lie in the range of pH 6.2 – 7.4, which encompasses the *in-vivo* pHe range of healthy and tumor tissue.²⁶ The pH sensing capability of MBA-AuNF, together with its spatial addressability and the biocompatible nature of the substrate, make it an excellent sensor to measure pHe in *in-vitro* cellular microenvironments.

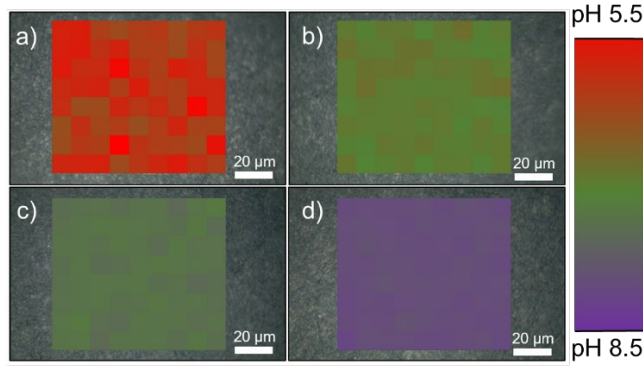


Figure 3. 90x80 μm pH map of MBA-AuNF surface at (a) pH 6, (b) pH 7, (c) pH 7.4 and (d) pH 8.

Table.1. Buffer pH compared to mean pixel pH of maps in Figure 3

Buffer pH	Sensor pH	SD (\pm)
6.00	5.93	0.25
7.00	6.97	0.08
7.40	7.38	0.06
8.00	7.99	0.04

Calibration of MBA-AuNF for pH sensing in the cellular microenvironment. The pH sensitivity of MBA is influenced by the chemical composition of the immediate environment of the sensor.⁹ To support HepG2/C3A cell growth, we treated the MBA-AuNF with collagen solution and submerged the substrate in cell culture media (DMEM). To ensure that pH measurements collected from the cellular microenvironment with MBA-AuNF were accurate, we re-calibrated the sensor post preparation for cell culture i.e. after incubation in collagen solution and DMEM. Figure 4a presents the calibration curve of MBA-AuNF pre- and post-preparation for cell culture.

We incubated the MBA-AuNF in type 1 collagen solution to create an extracellular environment that promoted cell adhesion. This process created collagen fibrils that coated the MBA-AuNF and formed bridges between adjacent fibers (Figure 4b and 4c). After coating MBA-AuNF in collagen and incubating with DMEM, the $I[\nu_s(\text{COO})]/I[\nu(\text{ref})]$ values at pH 6, 7, 7.2, and 8 increased, and the gradient of the calibration curve became steeper between pH 6 and 7.2 (Figure 4a). This had the benefit of increasing the resolution of the sensor in the physiological pH range, increasing the sensitivity of MBA-AuNF to the pHe

of cells. Figure 4a demonstrates the importance of calibrating SERS sensors under the same conditions as their intended application. The change in MBA-AuNF pH sensitivity is likely influenced by the collagen layer on the MBA-AuNF surface and the interaction of the MBA SAM with the complex chemical composition of DMEM. We utilize the post-collagen and DMEM exposure calibration curve of MBA-AuNF for all pH measurements we present in the following sections.

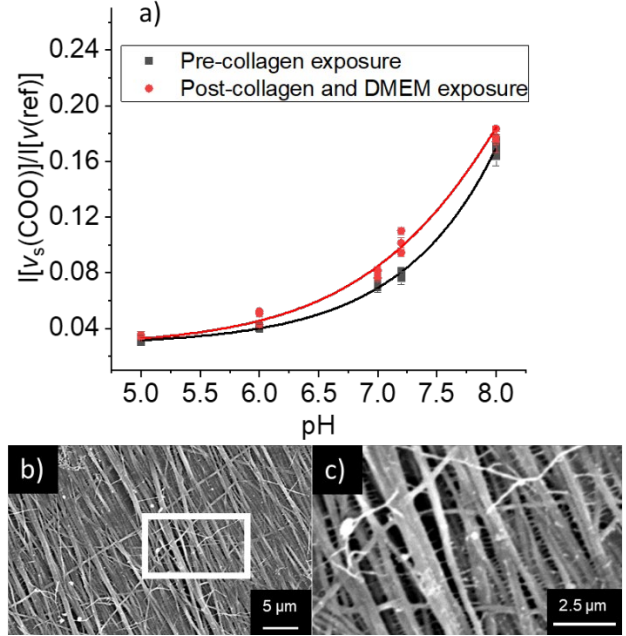


Figure 4. (a) MBA-AuNF pH calibration curve pre- and post-preparation for cell culture. (b) x3,000 SEM image of collagen fibrils bridging the larger MBA-AuNF fibers. (c) A zoomed-in frame of the area highlighted in (b).

Measuring pHe in the cellular microenvironment. We cultured HepG2/C3A on the MBA-AuNF surface and used SERS to measure pHe at the cell-fiber interface. HepG2/C3A is a carcinoma-derived cell line, and exhibits increased expression and activity of Na^+/H^+ exchangers and $\text{H}^+/\text{lactate}$ cotransporters, which contribute to the acidification of the tumor microenvironment *in-vivo*.³

SEM images confirmed that the HepG2/C3A cells form focal adhesion points with the fiber surface, and do not penetrate the dense fiber mesh (Figure 5). HepG2/C3A cells cultured on MBA-AuNF showed healthy morphology and developed microvilli-like structures on the cell membranes (Figure 5 and Figure S6).

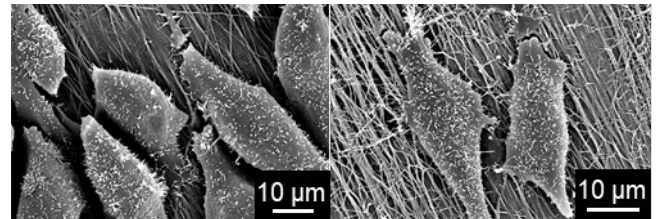


Figure 5. SEM images of HepG2/C3A cultured on MBA-AuNF.

By growing the HepG2/C3A on the surface of collagen-coated MBA-AuNF we can measure pHe in direct contact with the basolateral cell membrane using SERS (Figure S7). For pHe

measurements, we seeded a confluent layer of HepG2/C3A cells onto the MBA-AuNF surface. Figure 6a compares the pH we measured from MBA-AuNF with and without HepG2/C3A cultures on the substrate surface. In the absence of cells (Figure 6b), we recorded a pH of 7.22 ± 0.06 using MBA-AuNF, which is the pH of the PBS imaging solution. We confirmed the pH of the imaging solution was 7.18 ± 0.01 using a pH electrode. When we cultured HepG2/C3A cells to confluency on the MBA-AuNF (Figure 6c) we calculated a pH of 6.86 ± 0.06 from SERS spectra collected from the MBA-AuNF surface. This extracellular acidification is driven by proton and lactate secretion, the byproducts of HepG2/C3A cellular metabolism.³

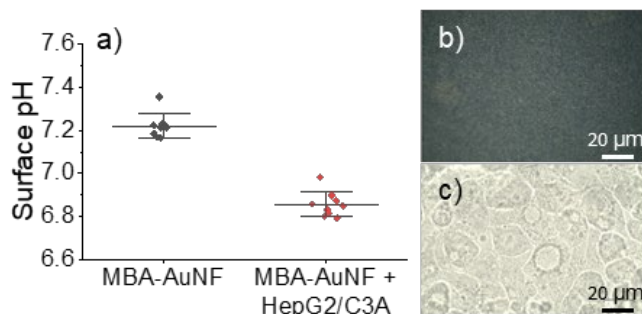


Figure 6. (a) MBA-AuNF surface pH with and without HepG2/C3A ($p < 0.01$, two-sample t-test). Each data point represents the mean of 9 spectra taken in a $150 \times 100 \mu\text{m}$ area (Figure S3), 3 data points were collected from different areas on 3 independent MBA-AuNF samples for each condition. (b) A blank MBA-AuNF submerged in the imaging solution. (c) A confluent HepG2/C3A monolayer on the MBA-AuNF surface.

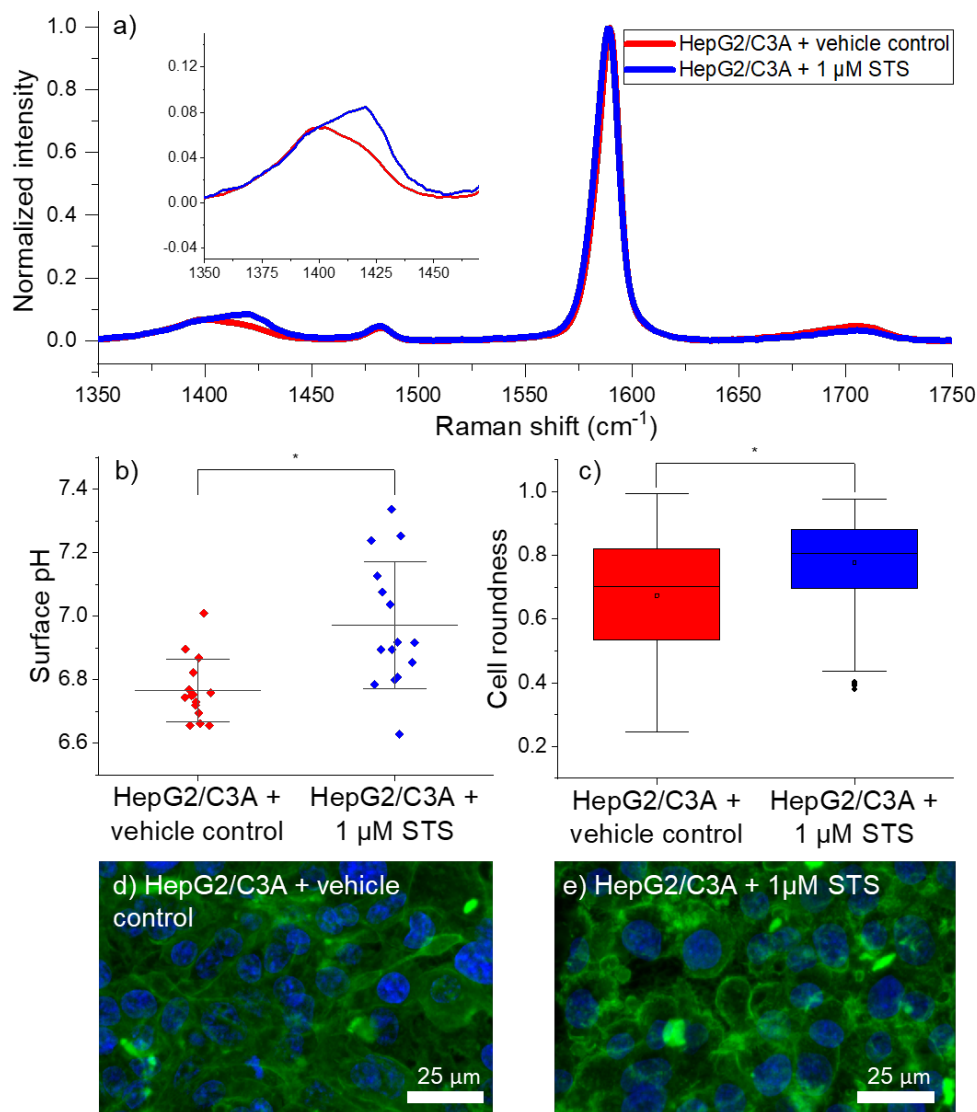
By supporting cell growth directly on its surface, MBA-AuNF is sensitive to local variations in pH that cannot be measured in cell cultures using a conventional pH meter. To demonstrate this we collected pH measurements from ~ 1 cm above cells cultured on MBA-AuNF using a conventional pH electrode (Figure S8). We detected no reduction in pH in the presence of HepG2/C3A using this method. This confirmed that the pH measurements in Figure 6 were made possible by the proximity and contact of MBA-AuNF with the HepG2/C3A basolateral surface.

Quantifying the impact of staurosporine on the HepG2/C3A pHe microenvironment. Staurosporine (STS) is a nonspecific protein kinase inhibitor that induces apoptosis in a wide range of cell lines.²⁸ Apoptosis plays a pivotal role in the pathogenesis of many diseases. Among these diseases is cancer, where a lack of apoptosis leads to the proliferation of malignant

cells upsetting the balance between cell division and cell death. Inducing apoptosis in tumors has been identified as a potential target for treatment.²⁹ The reverse pH gradient, acidic to basic, between the extracellular and intracellular space of tumor cells is implicated in the lower than expected efficacy of some cancer treatments *in-vivo*.³⁰ To this end, there is a need to understand how the pHe of the tumor microenvironment is influenced by apoptosis.

We investigated the impact of STS treatment on pHe by treating HepG2/C3A, cultured on MBA-AuNF, with $1 \mu\text{M}$ STS and a vehicle control solution (0.01% DMSO) for 3 hours. At the 3 hr time point, we measured a significant increase in cell rounding, a morphological hallmark of apoptosis, in brightfield images of samples treated with $1 \mu\text{M}$ STS (Figure 7c). We also observed F-actin reorganization, a key process in the early stages of apoptosis, and cell rounding, in fluorescence images of HepG2/C3A treated with $1 \mu\text{M}$ STS (Figure 7d and 7e).³¹

We collected SERS spectra from the cell-fiber interface of HepG2/C3A grown on MBA-AuNF to investigate the impact STS has on the pHe of the cellular microenvironment. Figure 7a presents the mean MBA-AuNF SERS spectrum collected from the basolateral surface of HepG2/C3A cells exposed to the vehicle control and the STS solutions for 3 hr. A clear increase in the intensity of $\nu_s(\text{COO})$ is visible in the samples treated with STS. This indicates that the pH at the cell-fiber interface is more alkaline after 3 hours of STS exposure. Figure 7b presents the pHe measured at 5 different locations from 3 vehicle control, and 3 STS treated HepG2/C3A cultures. We measured a pHe of 6.75 ± 0.10 in HepG2/C3A cultures treated with the control solution. Following 3 hours of exposure to STS, we measured an increase of 0.22 pH units in the mean pHe of HepG2-C3A cells. There was no loss of HepG2/C3A cell coverage after 3 hr of STS treatment, hence this increase in pH is not the result of a reduced cell population. We speculate this increase in pH is the result of reduced cell-fiber contact during cell rounding, or a decrease in Na^+/H^+ exchanger and $\text{H}^+/\text{lactate}$ cotransporter activity, which occurs during the early stages of apoptosis.¹ During apoptosis cells lose focal adhesion contacts with the extracellular environment, leading to cell rounding. In Figure 7d-e, there is an increase in cell rounding and reorganization of the actin skeleton in STS treated samples compared to control samples. This reduced contact between fibers and cell membrane could increase buffer flux to the fiber surface, raising local pH.³¹ Hence, using our novel MBA-AuNF sensors, we have correlated changes in cell morphology, which are associated with the early stages of apoptosis, to the pH microenvironment of HepG2/C3A, which is key to tumor pathogenesis.



CONCLUSION

We have developed a novel SERS substrate by leveraging the nanoscale dimensions of polymer fibers produced by the electrospinning process. While such an easily fabricated substrate with uniform SERS enhancement may have a wide range of applications in vibrational spectroscopy, we have chosen to demonstrate its utility as both a substrate for cell culture and a SERS platform for the measurement of localized pH variations. We have shown that when modified with a pH-responsive reporter (MBA), we can make precise pH measurements in a physiological range (5-8), and when cells are cultured on the surface of MBA-AuNF we can discriminate local changes in pH as a consequence of metabolic activity. Using this experimental approach we measured an increase in local pHe, after exposure

to protein kinase inhibitor STS, which correlated with morphological changes indicative of apoptosis. MBA-AuNF have great potential as a non-invasive method of collecting biological data, requiring no dye addition or staining. This low-impact sensing methodology could be integrated with microphysiological *in-vitro* platforms for non-invasive real-time monitoring of pHe, and help build a clearer understanding of the relationship between pHe and disease physiology.

ASSOCIATED CONTENT

Supporting Information.

Additional experimental details, cell viability assay, and images of HepG2/C3A on MBA-AuNF.

AUTHOR INFORMATION

Corresponding Author

Email: colin.campbell@ed.ac.uk

Author Contributions

The manuscript was written through contributions of all authors. WHS did all spectroscopy and cell culture. MC did all AuNF fabrication. SM fixed and prepared samples for SEM. AA provided support and protocols for cell culture of HepG2/C3A cells. RG, NR, AS, AA, KF and CJC all contributed to experimental and proof reading. All authors have given approval to the final version of the manuscript. ‡These authors contributed equally.

Notes

ACKNOWLEDGMENT

WHS and MC were supported by the EPSRC CDT in Intelligent Sensing and Measurement, Grant Number EP /L016753/1. AZ would like to thank Peter Newham for support in initiating the collaboration.

REFERENCES

1. Gottlieb, R. A., Cell acidification in apoptosis. *Apoptosis* **1996**, *1* (1), 40-48.
2. Parks, S. K.; Chiche, J.; Pouyssegur, J., Disrupting proton dynamics and energy metabolism for cancer therapy. *Nat. Rev. Cancer* **2013**, *13* (9), 611-23.
3. Cardone, R. A.; Casavola, V.; Reshkin, S. J., The role of disturbed pH dynamics and the Na⁺/H⁺ exchanger in metastasis. *Nat. Rev. Cancer* **2005**, *5* (10), 786-795.
4. Simonin, J.; Bille, E.; Crambert, G.; Noel, S.; Dreano, E.; Edwards, A.; Hattori, A.; Pranke, I.; Villeret, B.; Cottart, C.; Vrel, J.; Urbach, V.; Baatallah, N.; Hinzpeter, A.; Golec, A.; Touqui, L.; Nassif, X.; Galletta, L. J. V.; Planelles, G.; Sallenave, J.; Edelman, A.; Sermet-Gaudelus, I., Airway surface liquid acidification initiates host defense abnormalities in Cystic Fibrosis. *Sci. Rep* **2019**, *9* (1), 6516.
5. Gillies, R. J.; Raghunand, N.; Karczmar, G. S.; Bhujwalla, Z. M., MRI of the tumor microenvironment. *J. Magn. Reson. Imaging* **2002**, *16* (4), 430-450.
6. Chen, Y., Recent advances in fluorescent probes for extracellular pH detection and imaging. *Anal. Biochem* **2021**, *612*, 113900.
7. Yang, Y.; Xia, M.; Zhao, H.; Zhang, S.; Zhang, X., A Cell-Surface-Specific Ratiometric Fluorescent Probe for Extracellular pH Sensing with Solid-State Fluorophore. *ACS Sens* **2018**, *3* (11), 2278-2285.
8. Zhao, W.; Schafer, S.; Choi, J.; Yamanaka, Y. J.; Lombardi, M. L.; Bose, S.; Carlson, A. L.; Phillips, J. A.; Teo, W.; Droujinine, I. A.; Cui, C. H.; Jain, R. K.; Lammerding, J.; Love, J. C.; Lin, C. P.; Sarkar, D.; Karnik, R.; Karp, J. M., Cell-surface sensors for real-time probing of cellular environments. *Nat. Nanotechnol.* **2011**, *6* (8), 524-531.
9. Sun, F.; Zhang, P.; Bai, T.; David Galvan, D.; Hung, H.-C.; Zhou, N.; Jiang, S.; Yu, Q., Functionalized plasmonic nanostructure arrays for direct and accurate mapping extracellular pH of living cells in complex media using SERS. *Biosens* **2015**, *73*, 202-207.
10. Xu, M.; Ma, X.; Wei, T.; Lu, Z.-X.; Ren, B., In Situ Imaging of Live-Cell Extracellular pH during Cell Apoptosis with Surface-Enhanced Raman Spectroscopy. *Anal. Chem.* **2018**, *90* (23), 13922-13928.
11. Fleischmann, M.; Hendra, P. J.; McQuillan, A. J., Raman spectra of pyridine adsorbed at a silver electrode. *Chem. Phys. Lett* **1974**, *26* (2), 163-166.
12. Lee, S.; Chon, H.; Lee, J.; Ko, J.; Chung, B. H.; Lim, D. W.; Choo, J., Rapid and sensitive phenotypic marker detection on breast cancer cells using surface-enhanced Raman scattering (SERS) imaging. *Biosens* **2014**, *51*, 238-243.
13. Qian, X. M.; Nie, S. M., Single-molecule and single-nanoparticle SERS: from fundamental mechanisms to biomedical applications. *Chem. Soc. Rev.* **2008**, *37* (5), 912-920.
14. Reneker, D. H.; Yarin, A. L., Electrospinning jets and polymer nanofibers. *Polymer* **2008**, *49* (10), 2387-2425.
15. Kasani, S.; Curtin, K.; Wu, N., A review of 2D and 3D plasmonic nanostructure array patterns: fabrication, light management and sensing applications. *Nanophotonics* **2019**, *8* (12), 2065-2089.
16. Yang, T.; Ma, J.; Zhen, S. J.; Huang, C. Z., Electrostatic Assemblies of Well-Dispersed AgNPs on the Surface of Electrospun Nanofibers as Highly Active SERS Substrates for Wide-Range pH Sensing. *ACS Applied Materials & Interfaces* **2016**, *8* (23), 14802-14811.
17. Yu, M.; Dong, R.-H.; Yan, X.; Yu, G.-F.; You, M.-H.; Ning, X.; Long, Y.-Z., Recent Advances in Needleless Electrospinning of Ultrathin Fibers: From Academia to Industrial Production. *Macromolecular Materials and Engineering* **2017**, *302* (7), 1700002.
18. Keirouz, A.; Chung, M.; Kwon, J.; Fortunato, G.; Radacsi, N., 2D and 3D electrospinning technologies for the fabrication of nanofibrous scaffolds for skin tissue engineering: A review. *Wiley Interdiscip. Rev. Nanomed. Nanobiotechnol.* **2020**, *12* (4), e1626.
19. Kitsara, M.; Agbulut, O.; Kontziampasis, D.; Chen, Y.; Menasché, P., Fibers for hearts: A critical review on electrospinning for cardiac tissue engineering. *Acta Biomater.* **2017**, *48*, 20-40.
20. Grasl, C.; Bergmeister, H.; Stoiber, M.; Schima, H.; Weigel, G., Electrospun polyurethane vascular grafts: In vitro mechanical behavior and endothelial adhesion molecule expression. *J. Biomed. Mater. Res.* **2010**, *93A* (2), 716-723.
21. Jia, L.; Prabhakaran, M. P.; Qin, X.; Ramakrishna, S., Guiding the orientation of smooth muscle cells on random and aligned polyurethane/collagen nanofibers. *J. Biomater. Appl* **2014**, *29* (3), 364-377.
22. Bao, Y.; Lai, C.; Zhu, Z.; Fong, H.; Jiang, C., SERS-active silver nanoparticles on electrospun nanofibers facilitated via oxygen plasma etching. *RSC Advances* **2013**, *3* (23), 8998-9004.
23. Jaworska, A.; Jamieson, L. E.; Malek, K.; Campbell, C. J.; Choo, J.; Chlopicki, S.; Baranska, M., SERS-based monitoring of the intracellular pH in endothelial cells: the influence of the extracellular environment and tumour necrosis factor- α . *Analyst* **2015**, *140* (7), 2321-2329.
24. Schneider, C. A.; Rasband, W. S.; Eliceiri, K. W., NIH Image to ImageJ: 25 years of image analysis. *Nature Methods* **2012**, *9* (7), 671-675.
25. Lee, K. H.; Kwon, G. H.; Shin, S. J.; Baek, J.-Y.; Han, D. K.; Park, Y.; Lee, S. H., Hydrophilic electrospun polyurethane nanofiber matrices for hMSC culture in a microfluidic cell chip. *J. Biomed. Mater. Res.* **2009**, *90A* (2), 619-628.
26. Kraus, M.; Wolf, B., Implications of Acidic Tumor Microenvironment for Neoplastic Growth and Cancer Treatment: A Computer Analysis. *Tumor Biol.* **1996**, *17* (3), 133-154.
27. Wang, F.; Widejko, R. G.; Yang, Z.; Nguyen, K. T.; Chen, H.; Fernando, L. P.; Christensen, K. A.; Anker, J. N., Surface-Enhanced Raman Scattering Detection of pH with Silica-Encapsulated 4-Mercaptobenzoic Acid-Functionalized Silver Nanoparticles. *Anal. Chem.* **2012**, *84* (18), 8013-8019.
28. Belmokhtar, C. A.; Hillion, J.; Ségal-Bendirdjian, E., Staurosporine induces apoptosis through both caspase-dependent and caspase-independent mechanisms. *Oncogene* **2001**, *20* (26), 3354-3362.
29. Wong, R. S. Y., Apoptosis in cancer: from pathogenesis to treatment. *J. Exp. Clin. Cancer Res.* **2011**, *30* (1), 87.
30. Wojtkowiak, J. W.; Verduzco, D.; Schramm, K. J.; Gillies, R. J., Drug Resistance and Cellular Adaptation to Tumor Acidic pH Microenvironment. *Mol. Pharm.* **2011**, *8* (6), 2032-2038.
31. Desouza, M.; Gunning, P. W.; Stehn, J. R., The actin cytoskeleton as a sensor and mediator of apoptosis. *BioArchitecture* **2012**, *2* (3), 75-87.

For Table of Contents Only

